



**HAL**  
open science

# Swelling of Semi-Crystalline PVDF by a PMMA-based Nanostructured Diblock Copolymer: Morphology and Mechanical Properties

Evdokia Oikonomou, Sylvie Tencé-Girault, Pierre Gérard, Sophie Norvez

## ► To cite this version:

Evdokia Oikonomou, Sylvie Tencé-Girault, Pierre Gérard, Sophie Norvez. Swelling of Semi-Crystalline PVDF by a PMMA-based Nanostructured Diblock Copolymer: Morphology and Mechanical Properties. *Polymer*, 2015, 76, pp.89-97. 10.1016/j.polymer.2015.08.055 . hal-03822201

**HAL Id: hal-03822201**

**<https://hal.science/hal-03822201>**

Submitted on 20 Oct 2022

**HAL** is a multi-disciplinary open access archive for the deposit and dissemination of scientific research documents, whether they are published or not. The documents may come from teaching and research institutions in France or abroad, or from public or private research centers.

L'archive ouverte pluridisciplinaire **HAL**, est destinée au dépôt et à la diffusion de documents scientifiques de niveau recherche, publiés ou non, émanant des établissements d'enseignement et de recherche français ou étrangers, des laboratoires publics ou privés.

# Swelling of Semi-Crystalline PVDF by a PMMA-based Nanostructured Diblock Copolymer: Morphology and Mechanical Properties

Evdokia K. Oikonomou,<sup>†</sup> Sylvie Tencé-Girault,<sup>†</sup> Pierre Gérard,<sup>‡</sup> and Sophie Norvez<sup>\*,†</sup>

<sup>†</sup> Laboratoire Matière Molle et Chimie, ESPCI ParisTech, PSL Research University, 10 rue Vauquelin, 75005 Paris, France; E-mail: [sophie.norvez@espci.fr](mailto:sophie.norvez@espci.fr)

<sup>‡</sup> ARKEMA, Groupement de Recherche de Lacq, RN 117 F-64170 Lacq, France

## Abstract

The influence of a self-organizing diblock copolymer on the morphology, crystallinity and mechanical properties of a high molecular weight polyvinylidene fluoride (PVDF) is investigated. A spherically organized nanostructured diblock copolymer containing 25 wt% of soft acrylate block and 75 wt% of rigid polymethylmethacrylate (PMMA) is incorporated in PVDF in proportions varying between 12.5 and 70 wt% copolymer. DSC and DMA experiments prove the miscibility of the glassy PMMA block with the amorphous fraction of PVDF, whereas the soft block is fully segregated, preserving the nanostructuring of the diblock copolymer in the blend. Transmission electron microscopy and SAXS experiments show that the copolymer is confined into the inter-lamellar gallery of PVDF, giving rise to a swelling of the crystalline/amorphous lamellar morphology. The long period  $L_p$  varies from 120 Å in pure PVDF to 200 Å in the presence of 25 wt% copolymer. WAXS experiments and ATR spectroscopy show that the polar  $\beta$  polymorph is favoured in the blends and that the PVDF crystallinity is preserved. Tensile tests demonstrate a large improvement of the elongation at break, without significant loss of strength for samples containing lower amounts of copolymer.

## 1. Introduction

Binary blends of amorphous block copolymer A-B with homopolymer A have been extensively reported.<sup>1-7</sup> In case of blends where the diblock copolymer is relatively dilute, the B blocks aggregate, protected from the A homopolymer by the A blocks. The final ordered structures depend on interplay of the macrophase and microphase transitions. Van der Waals attractions between B cores promote macrophase separation of A-B domains and A homopolymer, while entropy of mixing tends to stabilize the dispersion of A-B aggregates into the A homopolymer. The resulting morphology depends on respective lengths of homopolymer and compatible block segment. The corresponding molecular weight ratio ( $\lambda = M_{A,homo}/M_{A,block}$ ) generally determines the degree of solubilization of the homopolymer into the block copolymer domain. When  $\lambda \ll 1$ , the short A homopolymer chains swell the A blocks domains, this regime is called the “wet brush”.<sup>8</sup> In the case  $\lambda \cong 1$ , the “dry brush” regime, the A homopolymer chains locate in between the A block domains. These two regimes lead to a microphase separation. When  $\lambda \gg 1$ , the macrophase separation between A-B block copolymer domains and A homopolymer dominates. The homopolymers considered were mostly polystyrene (PS), dispersed in PS-*b*-polybutadiene<sup>1,5,6</sup> or in PS-*b*-polyisoprene,<sup>2,7</sup> and polymethylmethacrylate (PMMA) in PMMA-*b*-PS.<sup>3,4</sup>

Only a relatively few other studies reported mixtures where the homopolymer H was different chemically from all of the copolymer segments but can form miscible blends with one of the blocks. This case differs from the well-studied A/A-B blend, as miscible but unlike H and A structures may involve an exothermic enthalpy of mixing acting as an additional thermodynamic driving force for solubilization. This is a powerful lever to stabilize self-assembled nanostructures. The favorite pair reported was poly(2,6-dimethyl-1,4-phenylene oxide), PPO, with PS (mixtures of PPO in PS-*b*-polyisoprene<sup>9</sup> or in PS based triblocks).<sup>10,11</sup>

Blends of a semi-crystalline homopolymer with diblock copolymers were mainly reported in the case of diblock copolymers containing a crystallizable moiety. Crystalline-amorphous copolymers exhibit morphologies produced by the interplay between microphase separation and crystallization of one block. The Nojima's group in particular has extensively described systems based on polycaprolactone, PCL, in mixture with PCL-*b*-polybutadiene (PCL-*b*-PB) or PCL-*b*-polyethylene.<sup>12-14</sup> In these studies, PCL-*b*-PB diblock copolymer and PCL homopolymer both crystallize, producing lamellar and spherulitic morphologies at low temperature. Above the melting

temperature of the crystallizable block, the phase behavior is the same as in binary blends of amorphous homopolymer/copolymer: depending on the  $\lambda$  ratio, the PCL homopolymer swells the PCL blocks of the PCL-*b*-PB domains, localizes in between the PCL domains or macroscopically phase-separates. Upon cooling down, the PCL homopolymer and the PCL block can crystallize. For low  $\lambda$  values, an alternating structure composed of crystalline lamellae (mixed crystals of PCL block and PCL homopolymer) and amorphous layers is favored. For higher  $\lambda$  values, a mosaic structure of two lamellar morphologies may be observed, each consisting in a PCL region and a PCL-*b*-PB region. In substance, depending on the relative molar mass of the homopolymer and diblock copolymer, the crystalline domains are macro-separated or not.

Blends of semi-crystalline polyvinylidenedifluoride (PVDF) with diblock copolymers are barely reported in the literature, all dealing with amorphous block copolymers containing a PMMA block. Indeed, the pair PVDF/PMMA has been a popular system for polymer mixing study for decades.<sup>15-20</sup> PMMA mixes exothermically with PVDF, giving rise to full miscibility in the melt state as well as in the amorphous phase below the melting point of PVDF.<sup>15</sup> This miscibility stems from intermolecular interactions between the carbonyl groups of PMMA, and the CF<sub>2</sub> and CH<sub>2</sub> groups of PVDF, by dipolar interaction and hydrogen bonding, respectively. Depending on the crystallization conditions, PVDF may present three common polymorphs, the non-polar  $\alpha$  phase, most readily obtained from the melt, and the polar  $\beta$  and  $\gamma$  phases.<sup>21,22</sup> The  $\beta$  phase in particular has attracted much interest because of its piezo- or pyroelectric properties. The crystallization of PVDF is strongly affected by the blending with PMMA. It has been shown that small concentrations of PMMA promoted the  $\beta$  crystalline phase formation, as a result of PVDF/PMMA specific interactions forcing the PVDF bonds to adopt *trans-trans* conformations.<sup>20</sup> Miscible PMMA may incorporate into the lamellar structure of PVDF, giving rise to an increase of the long period  $L_p$  of PVDF.<sup>23</sup> Beyond 55 wt% PMMA, both polymer chains remain miscible at the molecular level, no crystalline features are observed upon cooling from the melt.<sup>17</sup> Lee and co-workers examined the influence of the semi-crystalline homopolymer on the micro-domain structuration of a diblock copolymer in binary blends of low molecular weight PVDF and PS-*b*-PMMA or PMMA-*b*-PPFS-*b*-PMMA.<sup>24,25</sup> In both cases, the addition of PVDF (6 times shorter than the PMMA block) significantly disturbed the pre-existing micro-domain structure, resulting in a poorly ordered morphology. The isothermal crystallization of PVDF, at temperatures higher than the  $T_g$  of the

PMMA blocks, was shown to depend on space constraints, but the long period  $L_p$  of the PVDF homopolymer remained essentially unchanged after crystallization in the blend. Mixtures of PVDF and block copolymers based on PMMA have been developed for applications, with the aim of associating the mechanical properties of PVDF with the ones of the diblock copolymer. PMMA-*b*-polyoxyethylene has been shown to improve porous structure of PVDF membrane in lithium ion batteries<sup>26</sup> and PVDF to improve mechanical properties in PMMA-*b*-PSSA membranes for fuel cells.<sup>27-29</sup> Triblock copolymers also were shown to improve mechanical properties of PVDF.<sup>30</sup> In their work, Ruzette and Leibler observed by transmission electron microscopy that PVDF was confined between nanostructured PS-*b*-PB-*b*-PMMA aggregates composed of multiple soft shells, and that it retained its crystallinity, permeability and chemical stability. These studies directed towards applications mainly focused to conductivity properties, thermal and mechanical stability, and membrane morphology or crystallization behavior of PVDF were fairly or not described.

In all the above instances, structure and morphology of the binary blends were extensively described in cases a low molecular homopolymer was incorporated into a diblock or triblock structure. The influence of block copolymers blended with high molecular semi-crystalline homopolymers was mainly reported in terms of applicative properties.<sup>31</sup> Here, a diblock copolymer is incorporated into a high molecular weight PVDF. The diblock copolymer is composed of a glassy PMMA block fully miscible with the amorphous part of PVDF and a soft acrylate block which has no affinity for the PVDF. The influence of this self-assembling diblock copolymer on the structural, morphological and thermo-mechanical properties of PVDF is studied in detail. We show for the first time that a block copolymer retaining its nanostructuration may be confined in the lamellar gallery of PVDF, giving rise to synergistically driven enhanced mechanical properties.

## 2. Experimental Section

## 2.1. Materials and Sample Preparation

**Materials.** PVDF (Kynar 761A,  $M_w \sim 200$  kg/mol), the diblock acrylic copolymer P(BA-co-HEMA)-b-PMMA,  $M_w$  40 kg/mol (**DB**), composed of 75 wt% PMMA, 20 wt% PBA and 5 wt% HEMA, as well as the first block of this copolymer, P(BA-co-HEMA) (**B**), were kindly provided by ARKEMA. To promote subsequent crosslinking, which is not described in this work, the PBA block was copolymerized with hydroxyethyl methacrylate (HEMA), which can be easily reacted, for example, using dialdehydes or diisocyanates, leading to weakly swellable cross-linked films.<sup>32</sup> PMMA homopolymer ( $M_w$  15 kg/mol) and solvent, N-methylpyrrolidone (NMP) were purchased from Aldrich. Molecular weights of PMMA homopolymer and PMMA block in **DB** are comparable.

**Film preparation.** PVDF blend films were prepared by casting polymer solutions containing 70 wt% NMP after continuous stirring at 70 °C for 24h. The blends were cast onto PTFE substrates at 80 °C for 7 hours and then further dried in vacuum oven at 80 °C overnight. Blends containing PVDF and **DB** or **B** were denoted as PVDF/**DB**<sub>x</sub> or PVDF/**B**<sub>x</sub>, where x is the wt% of **DB** copolymer or **B** block. Three films were prepared for comparison, one of neat PVDF, one containing 18.5 wt% PMMA (PVDF/PMMA18.5) and one of neat **DB** copolymer.

For mechanical measurements, NMP solutions of the polymers were precipitated in excess water, to avoid traces of residual solvent that could impact the mechanical properties of the films. Thin films (~ 200-500 μm) were obtained by hot pressing under a pressure of 1 ton at 200 °C for 2 minutes.

## 2.2. Characterizations

### Attenuated total reflection (ATR)-FTIR measurements.

ATR-FTIR spectra were recorded using a Bruker-Tensor 37 FT-IR spectrophotometer equipped with a Gold engate ATR accessory, resolution 4 cm<sup>-1</sup>, scan number 32.

### X-Ray Scattering techniques.

Wide-angle X-Ray scattering (WAXS) experiments were performed at room temperature in transmission mode by using Cu K $\alpha$  radiation ( $\lambda = 1.54 \text{ \AA}$ ) from an X-Ray generator (XRG3D Inel) operating at 40 kV and 25 mA. WAXS patterns were collected with a curve position sensitive detector (CPS120 Inel) and fitted in a wide  $2\Theta$  range from  $5^\circ$  to  $65^\circ$ , using the Fityk 0.9.8 software<sup>33</sup> for crystal phase identification and crystallization ratio measurements. The degree of crystallinity  $\chi_c$  of PVDF in the films was calculated using the equation:

$$\chi_c(\text{WAXS}) = \frac{A_c}{(1-x)(A_c + A_a)} \times 100\%$$

in which  $A_c$  and  $A_a$  are the areas under fitted crystalline peaks and amorphous halo, respectively, and  $(1-x)$  the weight fraction of PVDF in the blends PVDF/DBx. Small Angle X-Ray Scattering (SAXS) curves were acquired at the SOLEIL synchrotron facilities, France, using the SWING beam line, wavelength  $\lambda = 0.83 \text{ \AA}$ . The sample-CCD camera distance was 4.53 m, the  $q$  range  $3.0 \times 10^{-3}$  to  $0.2 \text{ \AA}^{-1}$ . Samples were sandwiched between mica sheets. The reduction of the 2D datasets to 1D was achieved by radially averaging the raw data detector counts using a SOLEIL software, Foxtrot-Profiles. All SAXS intensities were normalized accounting for the background scattering as well as the sample thickness and were converted to absolute scale in  $\text{cm}^{-1}$  by comparison with H<sub>2</sub>O scattering.

**Differential scanning calorimetry (DSC).** DSC measurements were performed using a Q1000 series TA Instrument at a rate of  $10 \text{ }^\circ\text{C}/\text{min}$  under nitrogen flow, following temperature ramps from  $-100 \text{ }^\circ\text{C}$  to  $180 \text{ }^\circ\text{C}$ . At the end of the first heating, all samples were left at  $180 \text{ }^\circ\text{C}$  for 2 minutes before cooling.

The degree of crystallinity  $\chi_c$  of PVDF in the blends was calculated using the equation:

$$\chi_c(\text{DSC}) = \frac{\Delta H_f}{(1-x)\Delta H_f^*} \times 100\%$$

where  $\Delta H_f$  and  $\Delta H_f^* = 104.5 \text{ J/g}$  are the melting enthalpies of PVDF in the blends and in a PVDF with  $\chi_c = 100\%$ , respectively,<sup>34</sup> and  $(1-x)$  the weight fraction of PVDF in the blends PVDF/DBx.

**Dynamic mechanical analysis (DMA).** Temperature evolution of both storage and loss moduli of blend films was measured using a TA Instruments Dynamical Mechanical Analyzer (Q800), in film tension configuration. Samples were submitted to a  $2 \text{ }^\circ\text{C}/\text{min}$  temperature ramp from  $-100 \text{ }^\circ\text{C}$  to  $190 \text{ }^\circ\text{C}$  and to a sinusoidal tensile deformation, frequency 1 Hz, deformation 0.1 %.

**Scanning electron microscopy (SEM).** The surface morphology of the blends was observed with a Hitachi S3600 scanning electron microscope operating at 5 or 10 kV. Each sample was sputter-coated with gold prior to observation.

**Transmission electron microscopy (TEM).** Blend morphologies were observed using a CEM 902 Zeiss microscope operating under a voltage acceleration of 80 kV. Thin sections (50 nm) were cut from the blend films at  $-130\text{ }^{\circ}\text{C}$  using an ultra-cryomicrotome (Leica Ultracut) and stained in  $\text{RuO}_4$  vapors prior to observation.

**Mechanical properties.** The strain–stress behavior of the thin films was tested in an Instron tensile test apparatus at a crosshead speed of 5 or 500 mm/min, until break. Sample size: 13 mm effective length, 2.15 mm width, 300  $\mu\text{m}$  thickness. For each material, at least five replicate specimens were tested.

### 3. Results and discussion

#### 3.1. Miscibility of PVDF and DB acrylic copolymer

Films containing 75 wt% of PVDF and 25 wt% **B** or **DB** were prepared as described in the experimental part, and their surface examined by SEM. Figure 1A shows that the **B** block mainly composed of PBA is not miscible with PVDF, as evidenced by the large segregated domains. In contrary, the blend containing 25 wt% **DB** appears more miscible at the scale of the observation (Figure 1B). Apart the few irregularities apparent in the SEM image that may be associated to defects, the smooth surface attests to the homogeneous nature of the blend.

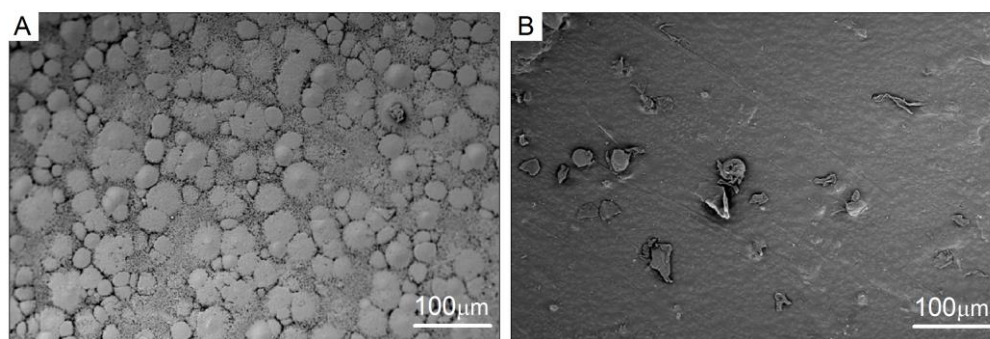


**Figure 1.** SEM images of A) PVDF containing 25 % **B** block; B) PVDF containing 25 % **DB** diblock copolymer.

The mechanical and thermal properties of the films were investigated to better evaluate the miscibility of PVDF and **DB**. Figure 2 presents the DSC thermograms of blend films containing various quantities of copolymer **DB**. Neat PVDF features a single melting peak at  $T_m = 164\text{ }^\circ\text{C}$  (Figure 2A). This thermal response suggests that the as-cast PVDF consists primarily of one crystal polymorph (presumably the  $\alpha$ -crystal structure)<sup>19</sup>. In the presence of diblock copolymer, the melting peak first shifts to a slightly higher temperature suggesting the presence of the higher melting  $\beta$ - or  $\gamma$ -crystal polymorphs promoted by the presence of the polar copolymer.<sup>19</sup> By increasing **DB** content, a pronounced melting point depression is observed, which is consistent with a favorable thermodynamic mixing of both polymers in the melt state and disruption of the PVDF crystallization.<sup>15,18,35</sup> Miscibility in blends including semi-crystalline components is achieved by the interaction between amorphous parts of each component. In case of PVDF/**DB**50 and PVDF/**DB**70, the  $T_m$  has shifted down to  $157\text{ }^\circ\text{C}$  and  $152\text{ }^\circ\text{C}$  respectively, comparable to those reported for solvent-cast PVDF/PMMA blends containing 56 % and 65 % of PMMA, respectively.<sup>15</sup>

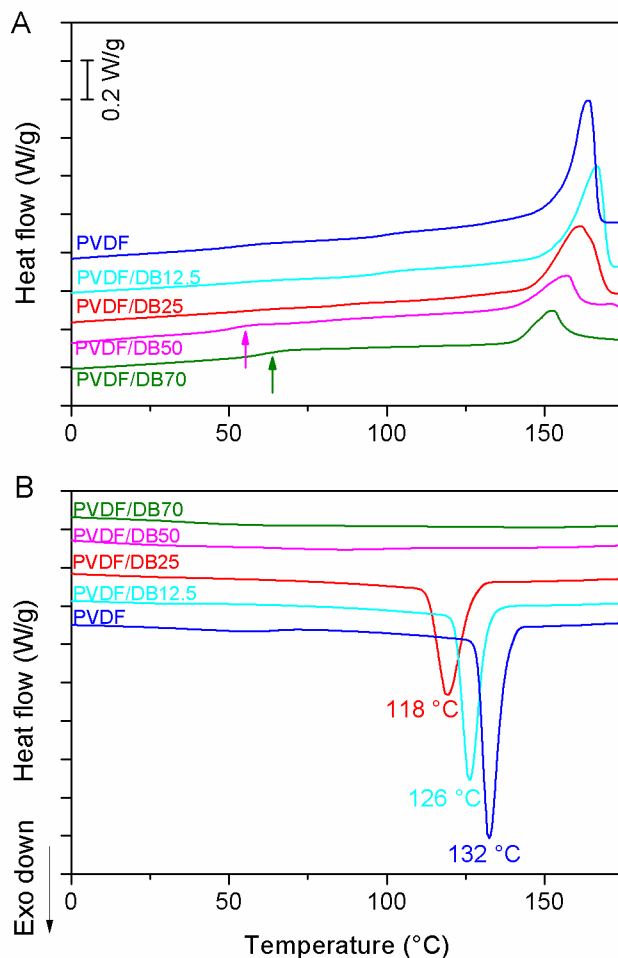


**Figure 2.** DSC thermograms of PVDF/**DB***x* thin films (*x* = 0, 12.5, 25, 50, 70), cast from NMP solutions evaporated at 80 °C. A) First heating ramp; B) cooling ramp. The arrows indicate  $T_g$  for PVDF/**DB**50 and PVDF/**DB**70 films.

Upon cooling from the melt, PVDF retains substantial crystalline content or remains in the amorphous state depending on melt composition (Figure 2B). The crystallization exotherm shifts to lower temperatures with increasing copolymer content, meaning that **DB** exerts a supercooling effect associated to a reduction of the crystallization rate. In **DB**-rich blends, the crystallization is completely disrupted resulting in a 100 % amorphous material. No crystallization is observed for blends with **DB** amount greater than 50 wt%, the same as for PVDF/PMMA blends prepared from the melt.<sup>20</sup>

By contrast, blends of PVDF with **B** block exhibit no  $T_m$  depression (Figure 3), as expected from the macrophase-separated structure. The melting point of PVDF is found at 165 °C for three

different compositions of PVDF/**B** (6.25 wt% **B** corresponds to the actual wt% of **B** block in the PVDF/**DB**25). This is in accordance with the non-miscibility of **B** block observed in the SEM image of Figure 1. Moreover, a slight increase of the crystallization temperature is observed by increasing **B**. Crystallization occurs at 140 °C in presence of 25 wt% **B** compared with 132 °C for pure PVDF. This suggests that the presence of the non-miscible component may act as a nucleating agent in the crystallization process of PVDF.

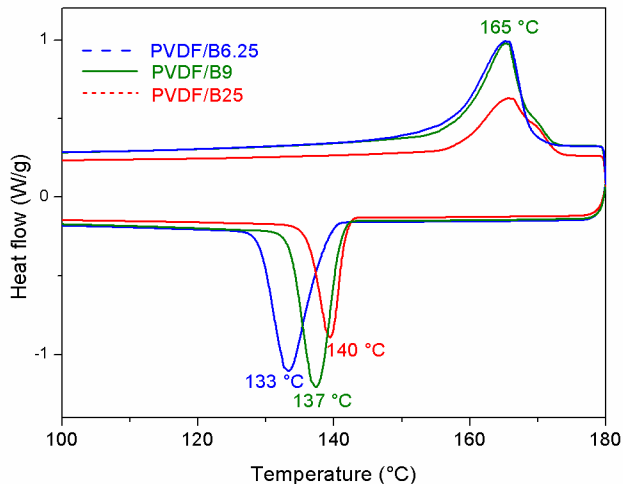


**Figure 3.** DSC thermograms of three PVDF/**B**<sub>x</sub> films containing 6.25, 9 and 25 wt% of the non-miscible **B** block. Heating-cooling rate 10 °C/min. The 6.25 wt% ratio corresponds to the actual ratio of **B** block in the PVDF/**DB**25.

The miscibility of PVDF and **DB** is also featured by the evolution of  $T_g$  which is visible on Figure 2A at least for PVDF/**DB**50 and PVDF/**DB**70 around 60 °C and 70 °C, respectively. The evolution of  $T_g$  is however better evidenced using dynamic mechanical analysis (DMA). The storage moduli  $E'$  and  $\text{Tan}\delta$  of different films are presented in Figure 4. The diblock copolymer shows a high storage modulus (>1000 MPa) until the glass transition temperature of PMMA where the modulus decreases abruptly (Figure 4A). Only 30% of the semi-crystalline PVDF present in PVDF/**DB**70 is enough to provide stiffness to the blend until the melting temperature  $T_m$  of PVDF at ca. 150 °C in the blend. As indicated by the arrow in Figure 4A, the modulus continuously increases by increasing the semi-crystalline fraction. Figure 4B shows for neat PVDF a relaxation temperature around -33 °C, which is assigned to the cooperative segmental motions within the main chains of the amorphous regions (the so-called  $\beta$  relaxation or  $T_g$ ). A second signal observed

around 90 °C is associated with various motions within the crystalline fraction ( $\alpha$  or  $\alpha_c$  relaxation).<sup>36</sup> Neat **DB** presents two  $T_g$  around 20 °C and 100 °C, attributed to the butyl acrylate block and PMMA block, respectively, confirming the incompatibility between blocks in the copolymer. In PVDF/**DB**70, the  $\text{Tan}\delta$  signal is not very different from the one of **DB**, except that the  $T_g$  corresponding to the PMMA block has shifted down to 90 °C. The  $T_g$  corresponding to the butyl acrylate block still occurs at 20 °C. This suggests partial miscibility with the amorphous PVDF acting essentially on the PMMA moiety of the copolymer. By decreasing **DB** ratio, the high  $T_g$  keeps on decreasing, from 90°C (PVDF/**DB**70) to 25°C (PVDF/**DB**12.5), supporting the fact that the PMMA block is miscible in the amorphous part of PVDF. By contrast, the low relaxation temperature, around -30 °C in neat PVDF, is not clearly affected in PVDF/**DB**12.5 and PVDF/**DB**25. Indeed, the low temperature signal of PVDF/PMMA blends is described in literature as composed of two contributions, one associated to the  $\beta$ -relaxation, affected by PMMA ratio, and another one ( $\alpha_a$ ) whose position is invariable with PMMA ratio, but which disappears for high amounts of PMMA when the blends are amorphous.<sup>37,38</sup> This  $\alpha_a$  relaxation is associated with motions in a crystal-amorphous interphase at the fold surface of PVDF crystalline lamellae, which cannot include PMMA for steric reasons. The low temperature signal observed around -30 °C in Figure 4B for PVDF/**DB**12.5 and PVDF/**DB**25 could be associated to this amorphous interphase. For PVDF/**DB**50, the broad signal between -70 °C and +20 °C can be understood as a merging of the  $\alpha_a$  relaxation of PVDF and  $T_g$  of the butyl acrylate block.

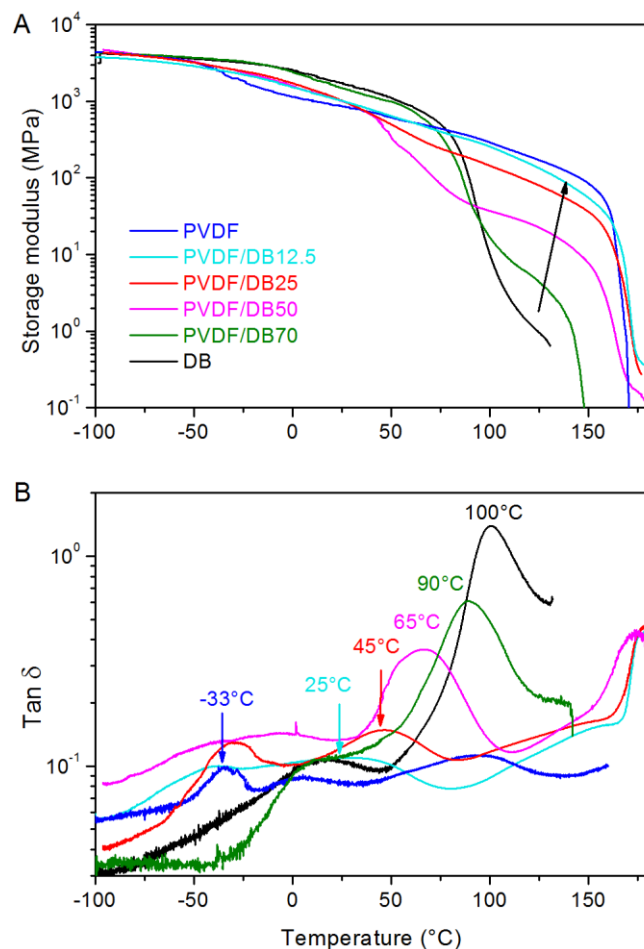


**Figure 4.** Evolution of A) the storage moduli  $E'$ ; B)  $\text{Tan}\delta$  of PVDF/DB $x$  blends as a function of temperature. The arrow in Figure A indicates the improvement of modulus by increasing the semi-crystalline fraction in the blend.

### 3.2. Phase morphology of the blends

**Transmission Electron Microscopy.** Figure 5 shows a collection of TEM micrographs of PVDF/DB $x$ , as well as neat PVDF (Figure 5A) and DB (Figure 5B) films. The thin sections have been treated with ruthenium tetroxide selectively staining the **B** block, which appears darker on the images. In neat PVDF, crystalline features can hardly be observed despite a crystallinity around 30 % (*vide infra*), due to the low contrast between amorphous and crystalline phases. The film of DB copolymer exhibits a nano-phase separation between blocks: domains of **B** (diameter ca. 6 nm)

are dispersed in the PMMA matrix. The average inter-domain distance is estimated at ca. 20 nm. In all **DB**-containing blends, the crystalline lamellar morphology of PVDF appears clearly, by contrast with neat PVDF. This is related to the presence of **DB** copolymer inside the amorphous lamellae of PVDF, in that the stained **B** block enhances the contrast between crystalline and amorphous parts of the sample. For blends containing 25 wt% and 50 wt% **DB**, the copolymer seems to be truly incorporated into amorphous lamellae, whereas for PVDF/**DB**70 large areas of nanostructured copolymer coexist with the lamellar structure of PVDF. Mixtures containing the non-miscible **B** block show completely different features (Figure 6): In PVDF/**B**25 film the **B** block is fully expelled from the PVDF lamella, forming pockets between bundles of lamellae, as already observed in PVDF/PMMA blend.<sup>39</sup>

In our system, the size of the block copolymer domains (< 20 nm) is comparable to the characteristic length  $L_p$  of the periodic crystal/amorphous PVDF organization. The miscibility of the PMMA block with the amorphous phase of PVDF allows for a confinement of the block copolymer in the amorphous lamellae, by contrast with PS-*b*-PB-*b*-PMMA/PVDF blends described by Ruzette and Leibler.<sup>30</sup> In their system, the core-shell aggregates formed by the triblock copolymer were larger (70 nm) than the  $L_p$  of PVDF and thus did not incorporate into the amorphous layers between crystalline lamellae of the homopolymer. PVDF intimately mixed with PMMA brushes remained confined between nanostructured objects. In our case, the nanostructured copolymer locates inside the lamellar gallery of PVDF. The spherulitic crystal/amorphous lamellae organization is preserved but swelled.

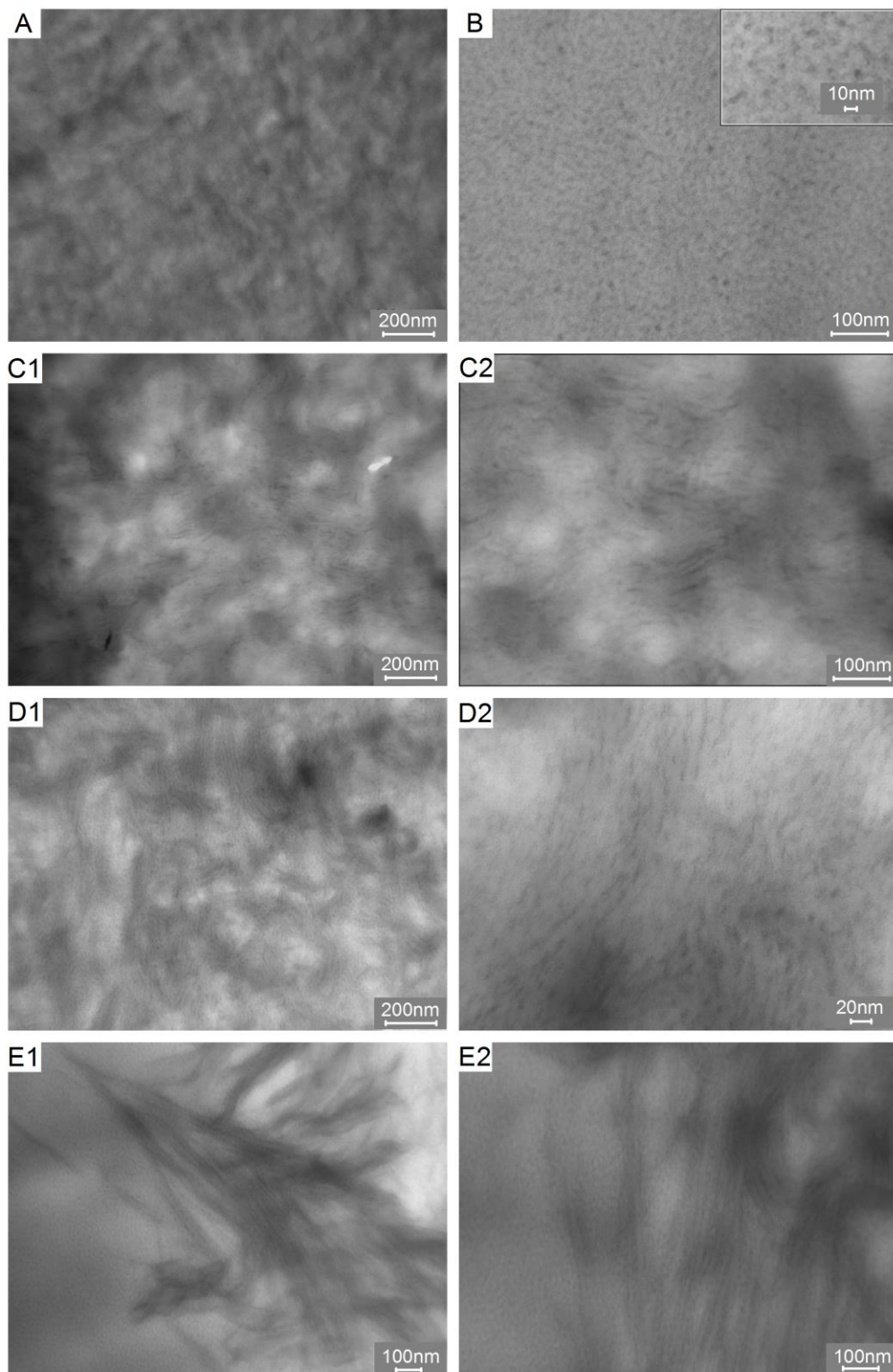


**Figure 5.** TEM images of A) neat PVDF; B) **DB**; C1,C2) PVDF/**DB**25; D1,D2) PVDF/**DB**50; E1,E2) PVDF/**DB**70. **B** block of the copolymer appears darker.

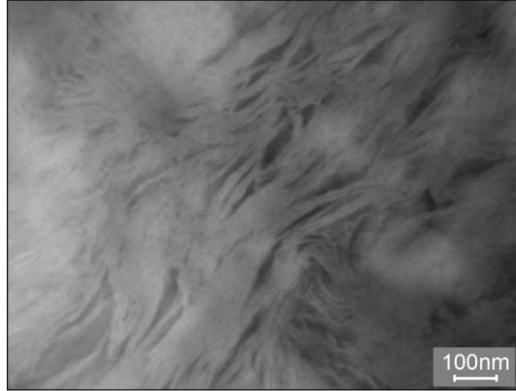


**Figure 6.** TEM image of macrophase-separated PVDF/DB25 blend.

**Small Angle X-Ray Scattering.** Figure 7 contains two representations of SAXS data for PVDF/DB $x$  blends as well as neat PVDF and DB copolymer. On the left, the  $\log I(q) = f(q)$  plot is the adequate representation for wide range scattering intensity systems, while the  $q^2 I(q) = f(q)$  representation (on the right) is used for isotropic lamellae organizations.

Figure 7A displays the SAXS profiles of solvent-cast films. Neat PVDF exhibits a weak scattering peak, the maximum of  $q^2 I(q)$  at  $q \sim 0.053 \text{ \AA}^{-1}$  giving rise to a PVDF long period  $L_p$  of 120  $\text{\AA}$ . The DB scattering shows a small peak located at 245  $\text{\AA}$  ( $q \sim 0.025 \text{ \AA}^{-1}$ ), a value consistent with the inter-domain distance previously observed by TEM (Figure 5B). The addition of DB into PVDF causes a significant increase of the scattering intensity as well as a gradual evolution of the scattering shape from a semi-crystalline lamellar scattering (PVDF/DB12.5) to a block copolymer domain scattering (PVDF/DB70). Specifically, the incorporation of small amounts of DB shifts peaks to lower angles, corresponding to increasing  $L_p$ , 136  $\text{\AA}$ , 200  $\text{\AA}$  for PVDF/DB12.5 and PVDF/DB25, respectively. This significant  $L_p$  increase indicates that copolymer chains are incorporated into amorphous PVDF, swelling the periodic crystalline lamellae. This is supported by the increase of scattering intensity in blends as compared with neat PVDF, due to preferential segregation of DB in the PVDF amorphous phase. Both electron densities of PBA and PMMA blocks (0.30 and 0.38  $e^-/\text{\AA}^3$ , respectively, as calculated using volume densities) are lower than that of amorphous PVDF (0.50  $e^-/\text{\AA}^3$ ). Insertion of DB copolymer in the amorphous PVDF lamellae thus enhances the electron density contrast between crystalline (0.59  $e^-/\text{\AA}^3$ ) and amorphous layers which results in a higher scattering intensity.

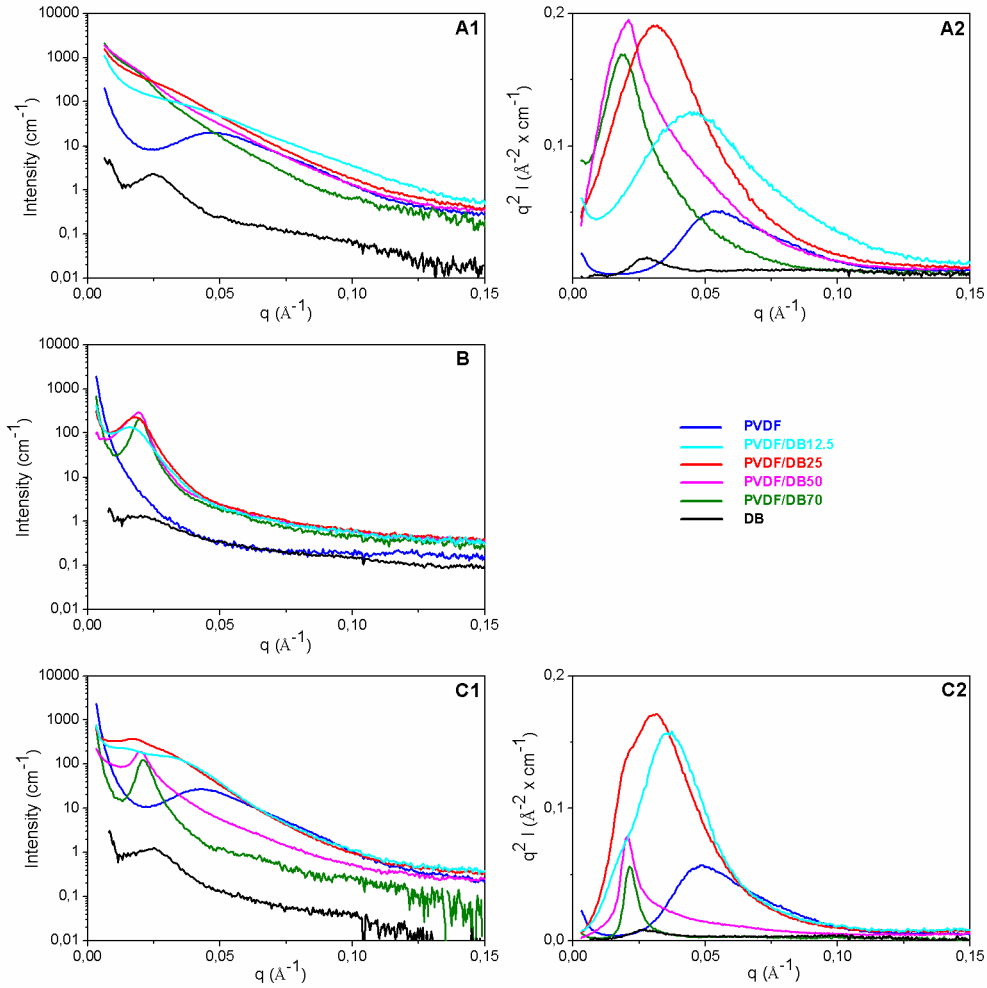


**Figure 7.** SAXS profiles of PVDF/DB $x$  films,  $x = 0, 12.5, 25, 50, 70, 100$ : A1,A2) solvent-cast. B) in the melt (186 °C).C1,C2) after cooling from the melt.1,  $\log I(q)$  plot; 2,  $q^2 I(q)$  plot.,

The SAXS profiles of PVDF/DB50 and PVDF/DB70 may be analyzed as the superposition of **DB** microphase-separated domains in amorphous PVDF, and crystalline lamellar organization of PVDF swelled by the nanostructured copolymer. For both blends, SAXS maxima appear in the small  $q$  range, corresponding to distances of 300 and 315 Å for PVDF/DB50 and PVDF/DB70, respectively, whereas the intensity of the scattering is also significant in the range of the swelled lamellae around  $0.05\text{Å}^{-1}$ . The superposition of both signals prevents the calculation of swelled  $L_p$  in these cases. The two different contributions are obvious in the  $q^2 I(q)$  plot in Figure 7-A2 and also visualized on the TEM pictures E1 and E2 in Figure 5.

To separate crystalline and copolymer scattering signals, samples were heated above the melting temperature of PVDF. Spectra acquired at 186 °C in the melt are reported in Figure 7B. As expected, the signal associated to the crystalline-amorphous contrast is no longer visible at 186 °C, due to the increased homogeneity of PVDF above the melting point. The scattering from the neat copolymer is very low, likely because the contrast between PBA and PMMA decreases above the glass temperature of PMMA. By contrast, in blends with PVDF, a significant scattering peak is observed when samples are heated to 186 °C, showing that the copolymer remains structured in the melted blend and/or that the contrast increases. The characteristic distance associated to this peak increases for decreasing amount of **DB**, from 320 Å for PVDF/**DB**70 to 390 Å for PVDF/**DB**12.5. This evolution is consistent with an isotropic dispersion of **DB** in melted PVDF. More PVDF mixed with PMMA moves the butyl acrylate cores apart.

SAXS experiments have been performed on samples crystallized from the melt after cooling at 12 °C/min (Figure 7C). Central diffusion seems to be lower in melt crystallized samples, perhaps because of the absence of residual solvent and a better homogeneity in these films. After melt crystallization, the neat PVDF long period is 130 Å and the swelling of the PVDF lamellar morphology is confirmed for the PVDF/**DB**12.5 and the PVDF/**DB**25, with long period of 168 Å and 200 Å, respectively. For the two other films, with higher content of **DB**, the main contribution in the spectra is the micellar scattering, only a very small lamellar signal due to crystallization is detected for the PVDF/**DB**50, and no crystallization behavior for the PVDF/**DB**70 (Figure 7C2), as already observed in DSC experiments (Figure 2B).

### 3.3. Crystallization of PVDF in thin blend films

The crystallization of the PVDF in the blend is strongly influenced by the presence of the block copolymer, which should impact the mechanical properties of thin films. The crystalline polymorphs in the PVDF/**DB** blends were identified using FTIR spectroscopy (ATR) and WAXS experiments, while the ratio of crystalline to amorphous phase was evaluated using DSC and WAXS (Table 1). WAXS and ATR spectra may be found in the Supplementary Information part (SI), for blends containing **DB** copolymer or **B** block. Figure 8 displays the WAXS pattern of PVDF/**DB**25 and the decomposition of the signal to amorphous and crystalline contributions. The WAXS acquisitions obtained with neat **DB** and PVDF (see WAXS spectra in Figure SI.1), enable

the evaluation of the shape of the amorphous halo of both **DB** and PVDF in the blends. To these amorphous contributions are superimposed the sharp crystalline peaks of PVDF. The integrated intensities of crystalline and amorphous parts, obtained after a refinement using the Fityk software, lead to the estimation of the crystalline ratios of the blend films as well as PVDF. From the position of the crystalline peaks, the  $\alpha$ ,  $\beta$  or  $\gamma$  polymorphs of PVDF may be identified.<sup>21</sup> For the PVDF/**DB**25 blend, the crystalline peak at  $\sim 4.3\text{\AA}$  ( $2\theta \sim 20.3^\circ$ ) corresponds to the  $d_{200}$  and  $d_{110}$  reticular distances of the  $\beta$  phase, while all the other sharp peaks are linked to the  $\alpha$  phase.

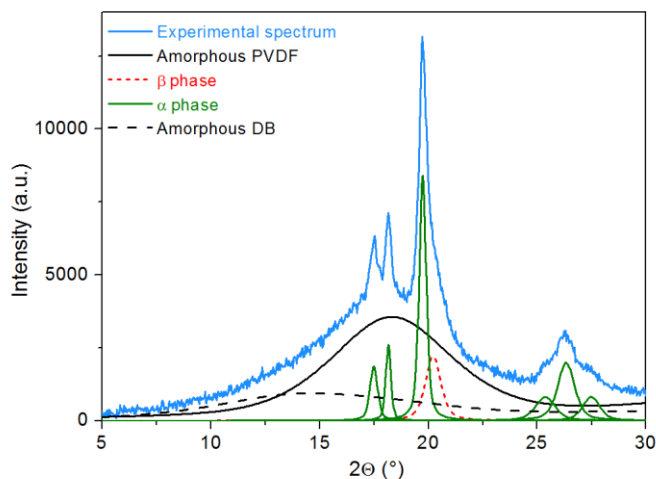


**Figure 8.** WAXS pattern of PVDF/**DB**25 as well as the decomposition in amorphous and crystalline contributions.

The film crystalline ratios  $\chi_c$  obtained from DSC and WAXS experiments are compared in Table 1. The crystalline index deduced from both methods are slightly different, but the same trend is observed. Whereas the crystalline ratio of the films decreases when the copolymer amount increases in the blend, the crystalline ratio of PVDF inside the blend is not significantly affected by the diblock incorporation. However the copolymer affects the crystalline phase of PVDF (see ATR spectra in Figure SI.2). For small amounts of **DB**, a mixture of  $\alpha$  and  $\beta$  phases is observed. The approximate proportion of each phase differs between ATR or WAXS data, likely related to a non-homogeneous distribution of the polymorphs inside the film. ATR is sensitive to surface composition while WAXS characterizes the whole sample. With increasing copolymer content (PVDF/**DB**50), the major crystalline polymorphs of PVDF are identified as the polar  $\beta$  and/or  $\gamma$ -form, an indication of **DB** miscibility with PVDF. For higher amounts of **DB**, the crystallinity of

the film is less than 10% and the polymorph may be identified only from WAXS experiment (the  $\alpha$  phase).

By contrast, the presence of 25 wt% of the non-miscible **B** block in the blend does not alter significantly the crystal phase of PVDF, which remains in the  $\alpha$  polymorph, as showed by ATR and WAXS (see SI). The retention of the  $\alpha$ -phase is likely associated to the macrophase-separation of phases in the blend.

**Table 1.** Melting temperatures  $T_m$  of PVDF in blends, crystallinity  $\chi_c$  of films and PVDF estimated by DSC and WAXS, PVDF polymorphs ( $\alpha$ ,  $\beta$ ,  $\gamma$ ) obtained from ATR and WAXS experiments (see SI). (+), (-) indicate the relative amount of each phase.

	$T_m$ (°C)	Film $\chi_c$		PVDF $\chi_c$		PVDF polymorph	
		DSC (%)	WAXS (%)	DSC (%)	WAXS (%)	ATR	WAXS
PVDF	164	35	27	35	27	$\alpha$	$\alpha$
PVDF/ <b>DB</b> 12.5	167	34	22	37	25	$\alpha(+)+\beta(-)$	$\beta(+)+\alpha(-)$
PVDF/ <b>DB</b> 25	161	29	20	38	27	$\alpha(+)+\beta(-)$	$\alpha(+)+\beta(-)$
PVDF/ <b>DB</b> 50	157	12	10	24	20	$\beta(+)+\gamma(+)$	$\beta(+)+\gamma(+)$
PVDF/ <b>DB</b> 70	152	11	9	35	28	-	$\alpha$
PVDF/ <b>B</b> 6.25	165	32		34		$\alpha$	
PVDF/ <b>B</b> 9	165	29		32		$\alpha$	
PVDF/ <b>B</b> 25	165	18	24	23	32	$\alpha$	$\alpha(+)+\beta(-)$

It is worthwhile to notice that the polar  $\beta$  polymorph of PVDF is actively sought as it presents unique dielectric and ferroelectric properties.<sup>21,40</sup> It is likely that the presence of the  $\beta$  phase as well as the swelling of the amorphous phase in our blends should induce dielectric changes that could be of interest. However the present work is limited to the study of the influence of these structural changes on the mechanical properties of the blends.

### 3.4. Mechanical properties of blend thin films

Blending of PMMA with PVDF commonly results in the decrease of tensile strength with only a slight influence on the elongation at break.<sup>41-43</sup> Song *et al.* recently described a series of tensile tests for the entire PVDF/PMMA composition range. The blend containing 40 % PMMA showed the lowest yield strength (24 MPa) and the highest elongation at break (> 750 %). Further increase of PMMA content caused a yield strength increase and a decrease of the elongation at break. As long as PVDF remains the major phase of the blend, decrease of the yield strength and increase of the elongation at break are jointly attributed to lower crystallinity, smaller spherulite size and formation of the  $\beta$  crystalline phase of PVDF. When PMMA becomes the major phase, the mechanical properties of the blend are dominated by the high strength and the low tensile strain of this glassy polymer.<sup>43</sup>

Here, the stress-strain characteristics of the PVDF/**DB**<sub>x</sub> films were recorded at two different crosshead speeds, 5 mm/min and 500 mm/min (Figure 9). A blend of PVDF with 18.5 wt% PMMA, corresponding to the amount of PMMA in PDVF/**DB**25 blend, was also tested for comparison. At low speed (Figure 9A), the elongation at break is higher than that of neat PVDF for compositions up to 50 wt% **DB**. The blend PVDF/**DB**70 presents a much lower elongation at break in accordance with the elevated amount of glassy PMMA (~50%). The PVDF/**DB**25 blend presents the same stress-strain behavior as PVDF/PMMA18.5. When the crosshead speed is increased up to 500 mm/min, the difference between the blends containing PMMA or **DB** becomes more pronounced (Figure 9B). The three blends containing 12.5, 25 and 50 wt% copolymer present a large elongation at break (> 550 %) which is limited for PVDF/PMMA18.5 (200 %). For PVDF/**DB**12.5 blend in particular, the elongation is the highest without significant loss of modulus. This increase in break elongation is likely related to the presence of the soft **B** block incorporated in the amorphous phase of PVDF. At room temperature the **B** block is above its glass transition, and forms soft inclusions, providing an improvement in molecular mobility, and therefore enhanced ductility. With only 12.5 wt% **DB**, the blend presents improved mechanical properties at both speeds, with good yield strength and high elongations at rupture. This behavior, especially noticeable at high speed, suggests improved impact strength for the PVDF/**DB** system versus PVDF/PMMA blend materials that should be the subject of a future work.

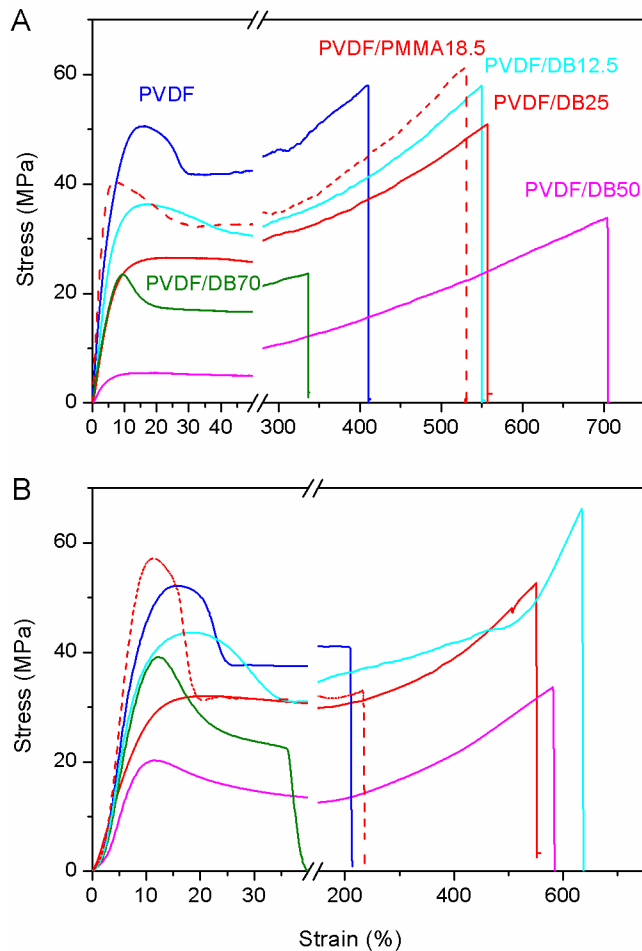


**Figure 9.** Stress-strain experiments on blends PVDF/DB $x$ , neat PVDF and PVDF/PMMA18.5 at A) 5 mm/min; B) 500 mm/min.

#### 4. Conclusions

A diblock copolymer containing a soft acrylate block and a glassy PMMA block (75 wt% PMMA), which self-organizes in 6-nm cores of soft acrylate block in the matrix of PMMA, was blended with high molecular weight PVDF in proportions varying between 12.5 and 70 wt% copolymer. DSC and DMA experiments prove the miscibility of the PMMA block with the amorphous part of PVDF, whereas the soft acrylate block is fully expelled. The PMMA component of the diblock copolymer acts as an efficient intercessor for dispersing PBA moiety in PVDF. The crystallinity and lamellar morphology of PVDF are preserved in the blends, and a gradual swelling of the

crystalline/amorphous lamellae organization is observed by increasing the amount of copolymer. The microphase-separated domains of the copolymer are confined into the amorphous lamellar gallery of PVDF, owing to the size of the spherical nano-objects which fit the long period  $L_p$  of PVDF. Tensile tests showed a 3-fold improvement of the elongation at rupture in presence of the copolymer, without significant loss of strength for the blends containing low levels of diblock copolymer. Hence, the intimate mixing of the semi-compatible diblock copolymer in PVDF is a powerful tool to impart the resultant material with superior combination of mechanical properties. This improvement is notably visible at high speed and should be associated to an improved impact strength which is crucial for many commercial applications.

**Acknowledgements.** Authors acknowledge SOLEIL for providing synchrotron radiation facilities and especially Dr. Pierre Roblin for his assistance in using the SWING beam line. They are also grateful to the LEM laboratory (ARKEMA, Serquigny France) for facilitating X-ray scattering experiments. Dr. François Beaume, Dr. Michel Glotin and Pr. Ludwik Leibler are warmly thanked for fruitful discussions.

### Supplementary Information

WAXS spectra of PVDF, PVDF/**DB50** and **DB** (SI.1) and ATR spectra of PVDF/**DBx**, PVDF and **DB** (SI.2).

### References

- 
- (1) Hashimoto, T.; Koizumi, S.; Hasegawa, H.; Izumitani, T.; Hyde, S. T. *Macromolecules* **1992**, *25*, 1433–1439.
  - (2) Koizumi, S.; Hasegawa, H.; Hashimoto, T. *Macromolecules* **1994**, *27*, 6532–6540.
  - (3) Prahsarn, C.; Jamieson, A. M. *Polymer* **1997**, *38*, 1273–1283.
  - (4) Lowenhaupt, B.; Steurer, A.; Hellmann, G. P.; Gallot, Y. *Macromolecules* **1994**, *27*, 908–916.
  - (5) Roe, R.-J.; Zin, W.-C. *Macromolecules* **1984**, *17*, 189–194.
  - (6) Kinning, D. J.; Winey, K. I.; Thomas, E. L. *Macromolecules* **1988**, *21*, 3502–3506.
  - (7) Spontak, R. J.; Smith, S. D.; Ashraf, A. *Macromolecules* **1993**, *26*, 5118–5124.

- 
- (8) Koizumi, S.; Hasegawa, H.; Hashimoto, T. *Makromol. Chem. Macromol. Symp.* **1992**, *62*, 75–91.
- (9) Hashimoto, T.; Kimishima, K.; Hasegawa, H. *Macromolecules* **1991**, *24*, 5704–5712.
- (10) Tucker, P. S.; Barlow, J. W.; Paul, D. R. *Macromolecules* **1988**, *21*, 2794–2800.
- (11) Kim, J. K.; Jung, D. S.; Kim, J. *Polymer*, **1993**, *34*, 4613–4624.
- (12) Nojima, S.; Kuroda, M.; Sasaki, S. *Polym. J.* **1997**, *29*, 642–648.
- (13) Akaba, M.; Nojima, S. *Polym. J.* **2006**, *38*, 559–566.
- (14) Gondo, S.; Osawa, S.; Sakurai, T.; Nojima, S. *Polymer* **2013**, *54*, 6768–6775.
- (15) Nishi, T.; Wang, T. T. *Macromolecules* **1975**, *8*, 909–915.
- (16) Bernstein, R. E.; Cruz, C. A.; Paul, D. R.; Barlow, J. W. *Macromolecules* **1977**, *18*, 681–686.
- (17) Léonard, C.; Halary, J. L.; Monnerie L. *Macromolecules* **1988**, *21*, 2988–2994.
- (18) Sasaki, H.; Bala, P. K.; Yoshida, H.; Ito, E. *Polymer* **1995**, *36*, 4805–4810.
- (19) Ma, W.; Zhang, J.; Wang, X.; Wang, S. *Appl. Surf. Sci.* **2007**, *253*, 8377–8388.
- (20) Halary, J. L.; Jarray, J.; Fatnassi, M.; Ben Cheikh Larbi, F. *J. Eng. Mat. Technol.-Trans. ASME* **2012**, *134*, 010910.
- (21) Lovinger, A. J. In: *Developments in Crystalline Polymers*; Bassett, D. C., Ed.; Applied Science Publishers: London, **1982**; Chapter 5.
- (22) Gregorio, Jr., R.; Sousa Borges, D. *Polymer* **2008**, *49*, 4009–4016.
- (23) Fatnassi, M.; Larbi, F. B. C.; Halary, J. L. *Int. J. Pol. Sci.* **2010** (2010), Article ID 829752
- (24) Lee, J. K.; Kim, J. S.; Lim, H. J.; Lee, K. H.; Jo, S. M.; Ougizawa, T. *Polymer* **2006**, *47*, 5420–5428.
- (25) Kim, G. S.; Kang, M. S.; Choi, M. J.; Kwon, Y. K.; Lee, K. H. *Macromol. Res.* **2009**, *17*, 757–762.
- (26) Xiao, Q.; Wang, X.; Li, W.; Li, Z.; Zhang, T.; Zhang H. J. *Memb. Sci.* 2009, *334*, 117–122.
- (27) Chen, N.; Hong, L. *Polymer* **2004**, *45*, 2403–2411.
- (28) Choi, W. H.; Jo, W. H. *J. Power Sources* **2009**, *188*, 127–131.
- (29) Erdogan, T.; Unveren, E. E.; Inan, T. Y.; Birkan B. *J. Memb. Sci.* **2009**, *344*, 172–181.
- (30) Ruzette, A. V.; Leibler, L. *Nature Materials* **2005**, *4*, 19–31.
- (31) Court, F.; Leibler, L.; Mourran, A.; Navarro, C.; Royackkers, V.; *US Patent* **2006**, US 7,144,952 B1

- 
- (32) Gibon, C. M.; Norvez, S.; Iliopoulos, I.; Goldbach, J. T. *Eur. Pol. J.* **2008**, *44*, 1843–1848.
- (33) Wojdyr, M. *J. Appl. Cryst.* **2010**, *43*, 1126–1128.
- (34) Nakagawa, K.; Ishida, Y. *J. Polym. Sci. Part B: Polym. Phys.* **1973**, *11*, 2153–2171.
- (35) Gibon, C. M.; Norvez, S.; Tencé-Girault, S.; Goldbach, J. T. *Macromolecules* **2008**, *41*, 5744–5752.
- (36) Mano, J. F.; Sencadas, V.; Mello Costa, A.; Lanceros-Méndez, S. *Mater. Sci. Engin. A* **2004**, *370*, 336–340.
- (37) Hahn, B.; Herrmann-Schönherr, O.; Wendorff, J. *Polymer* **1987**, *28*, 201–208.
- (38) Mijovic, J.; Sy, J.-W.; Kwei, T. K. *Macromolecules* **1997**, *30*, 3042–3050.
- (39) Okabe, Y.; Murakami, H.; Noboru Osaka, N.; Saito, H.; Inoue, T. *Polymer* **2010**, *51*, 1494–1500.
- (40) Sharma, M.; Madras, G.; Bose, S. *Phys. Chem. Chem. Phys.* **2014**, *16*, 14792–14799.
- (41) Linares, A.; Acosta, J. L. *Eur. Polym. J.* **1997**, *33*, 467–473.
- (42) Pawde, S. M.; Deshmukh, K. *J. Appl. Polym. Sci.* **2009**, *114*, 2169–2179.
- (43) Song, H.; Yang, S.; Sun, S.; Zhang, H. *Polym-Plast. Technol. Engin.* **2013**, *52*, 221–227.